Implantable Miniaturized Glucose Fuel Cell

Hoai Chau Nguyen Van

Electrical Engineering and Computer Sciences
University of California at Berkeley

Technical Report No. UCB/EECS-2012-249
http://www.eecs.berkeley.edu/Pubs/TechRpts/2012/EECS-2012-249.html

December 14, 2012

Implantable Miniaturized Glucose Fuel Cell

by Hoai Chau Nguyen Van

Research Project

Submitted to the Department of Electrical Engineering and Computer Sciences, University of California at Berkeley, in partial satisfaction of the requirements for the degree of **Master of Science, Plan II**.

Approval for the Report and Comprehensive Examination:

Committee:

Professor Elad Alon
Research Advisor

Dec. 13th 2012

(Date)

* * * * * * *

Professor Michel Maharbiz
Second Reader

Dec. 13th 2012

(Date)

Acknowledgment

I would like to thank several people without whom this research has not been possible. Firstly, I would like to thank my research and academic advisor, Professor Elad Alon for giving me the opportunity to work in his lab at the Berkeley Wireless Research Center. I am thankful for his continual support, guidance, mentorship and most of all his patience. I would also like to thank Professor Michel Maharbiz for his thoughtful discussions and mentorship. Special thanks to Hanh-Phuc Le, my project teammate for all his help and support over the past few years. Last but not least, I'd like to thank everyone in Elad's group, Michel's group, and all BWRC staff, students and sponsors for their invaluable help and support.

Abstract

The growth of power-constrained bio-medical and sensor applications has kindled increasing interest in energy-harvesting methods. Direct glucose fuel has emerged as a candidate of choice due to reliability and safety advantages. In this thesis, a 1mm2 miniaturized direct fuel cell is presented. The fuel cell provides a peak power density of 0.34uW/cm^2 with an open voltage potential of 300mV. An analytical framework for the fuel cell as well as an example application in body touch interfaces will also be presented.

List of Figures

Contents

1

Introduction: Glucose Fuel Cell

1.1 Motivation

Power has increasingly become a limiting factor in the operation of electronics. For power-constrained devices such as biomedical implants, the need for power is especially important. Conventional batteries suffer from several key disadvantages, including the need for replacement, size, and weight. There is an increasingly large class of biomedical sensors and actuators that need to be powered such as brain machine interfaces [1,2,3], heart-rate pacemakers, or cochlear implants [4]. Another emerging class of devices involves body interface devices such as touch sensors on skin that would allow users to interact with the built environment in novel ways. For such devices, energy-harvesting methods are often required to eliminate the need for energy storage or routine replacement of batteries.

Several energy-harvesting methods have been developed that are specifically applicable in a biomedical implant environment such as thermoelectricity [5], piezoelectricity [6], radio-frequency inductive power transfer [7], and glucose fuel cells [8,9,10]. Thermoelectricity makes use of the thermal gradient that exists in the body. Piezoelectricity harvests energy from the body's movements, and RF inductive power transfer works via electromagnetic waves like those used in RFIDs. These methods suffer from several disadvantages such as output power reliability as well as safety. Specifically, fully implanted devices do not see large thermal gradient in the body, whereas the piezoelectricity method suffers from intermittent output. The use of RF inductive power for energy transfer leads to difficulties with practical deployment, since the RF energy source must be near the implant in order to avoid health risks from excessive radiation and/or exceedingly poor power transfer efficiency.

Due to the disadvantages of the other three methods for harvesting energy within the body, recently there have been considerable interests on the development of alternate methods such as glucose fuel cells, which are safer and have more reliable output power. Glucose fuel cells are highly desirable for biomedical implant applications because of the abundance of glucose in the body. The focus of this thesis is on a variant of glucose fuel cells called a direct glucose fuel cell, which uses non-enzymatic materials such as Platinum as catalysts. Direct glucose fuel has been successfully developed by several research groups such as in [8] and [9], and offers the potential for longevity as compared with other types of glucose fuel cells. However, in the literature, there has been a lack of existing work that focuses on the fabrication and assembling techniques that allows the miniaturization to make these fuel cells applicable to mm-scale implants.

The aim of this thesis is to address the miniaturization and low-cost prototyping of such devices as well as provide an analysis on an example application for such miniaturized devices. The organization of this thesis is as follows: Chapter 1 provides an introduction to glucose fuel cells, including the various types and alternatives. Chapter 2 offers an analytic study of the stacked structure of the direct fuel cell. Chapter 3 explains the design and fabrication of the miniaturized glucose fuel cell. Chapter 4 describes the experimental procedures and our obtained results for the fuel cell performance as well as the cell longevity. Chapter 5 provides the description of an example application for such miniaturized glucose fuel and design considerations for its associated circuitry.

1.2 What are Fuel Cells?

Fuel cells are electrochemical devices that directly convert chemical energy in fuel to electricity via a chemical reaction with oxygen. In contrast to battery cells, which are closed systems, fuel cells are open system where reactants flow or diffuse into the system instead of being stored within the cell. Catalysts are usually required to speed up the reactions as fuel cell reactions take place slowly on their own.

A well-known example of the fuel cell is the Hydrogen Fuel Cell, which is currently being explored as a power source for automobiles. Here, hydrogen indirectly reacts with oxygen to yield electron flow. The two half-cell equations for the hydrogen fuel cell are as follows:

$2H_2 \rightarrow 4H^+ + 4e^-$ $\quad E^o = 0.00V$ $\quad$ (Catalyst = Pt)

$4H^+ + O_2 + 4e^- \rightarrow 2H_2O$ $\quad E^o = 0.68V$ $\quad$ (Catalyst = Ni)

Overall: $2H_2 + O_2 \rightarrow 2H_2O$

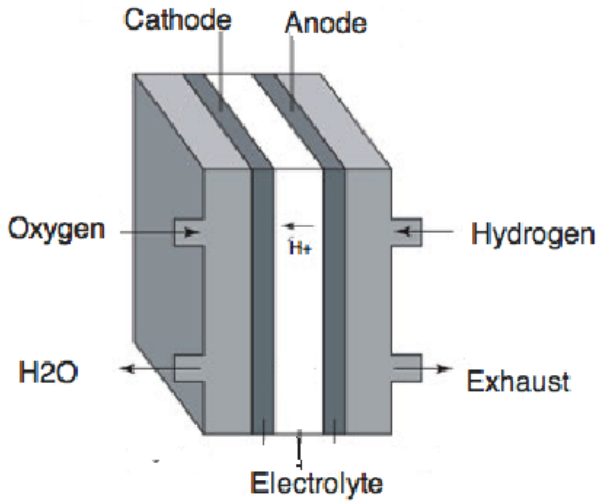

Figure 1.1 Hydrogen Fuel Cell. Adapted from [16]

As shown in Figure 1.1, the reactants are separated and are introduced into the cell via different inlets/outlets. On the anode side, hydrogen splits to yield protons and electrons, catalyzed by Platinum. On the cathode side, oxygen reacts with protons to yield water, consuming electrons in the process. The catalyst for the reaction at the cathode is Nickel. Overall the cell gives an external open-circuit voltage of 0.68V.

The above-described reactions happen for fuel cells with acidic electrolytes such as proton exchange membrane fuel cells or phosphoric acid fuel cells. Fuel cells with basic electrolytes have slightly different half-cell reactions (mediated by OH^- and not H^+), although the overall reaction is the same.

$$2H_2 + 4OH^- \rightarrow 4H_2O + 4e^-$$

$$2H_2O + O_2 + 4e^- \rightarrow 4OH^-$$

$$\text{Overall: } 2H_2 + O_2 \rightarrow 2H_2O$$

1.3 Glucose Fuel Cell

Glucose fuel cells are fuel cells in which the fuel is glucose. Glucose is readily available in biological systems such as in the tissue fluid or in the blood. The concentration of glucose in the tissue fluid is typically 5mM, whereas the oxygen concentration is typically 7%. In the glucose fuel cell, glucose indirectly reacts with oxygen to form oxidized products and water. When the oxidation is complete, CO_2 and water are the resultant byproducts. However, most frequently, glucose is first oxidized to yield gluconic acid, which might undergo further oxidation. The two half-cell equations are shown below:

At the anode (negative): $C_6H_{12}O_6 + H_2O \longrightarrow C_6H_{12}O_7 + 2H^+ + 2e^-$

At the cathode (positive): $\frac{1}{2}O_2 + 2H^+ + 2e^- \longrightarrow H_2O$

Overall reaction: $C_6H_{12}O_6 + \frac{1}{2}O_2 \longrightarrow C_6H_{12}O_7$

The potential of the cell is the difference in electrochemical potential of the anode and cathode redox pairs. Overall, the glucose fuel cell open-circuit voltage can reach 1.2V under standard conditions. Glucose fuel cells are exciting candidates for biomedical implantable devices due to its potential for reliability as well as the abundant availability of reactants in the tissue (glucose and oxygen) and its non-toxicity.

1.4 Type of Glucose Fuel Cells

There are three major types of glucose fuel cells, classified based on the type of catalyst used. The first type is an enzymatic glucose fuel cell, which uses biological enzymes such as glucose oxidase as catalysts. Enzymes are proteins by nature. As such they have limited long-term stability as changes in temperature and pH conditions can easily cause the denaturation of enzymes. However, enzymes have high reactant specificity and high reaction rate. This is advantageous as this limits any side-reaction.

The second type of glucose fuel cell is a microbial glucose fuel cell. These are fuel cells in which the catalysts are immobilized bacteria capable of oxidizing glucose. The greatest disadvantage of microbial glucose fuel cell is that there is a risk of infection due to bacteria escaping from the cell to other parts of the body. In addition, it is difficult to maintain stable microbe population.

Lastly, the third type of glucose fuel cell is the direct glucose fuel cell first reported by Warner and Robinson in 1967 [11]. Also known as abiotic fuel cells, they are fuel cells that use inorganic catalysts. For the cathode, which is required to be oxygen-selective, platinum alloys or activated carbon can be employed [8,9,10]. Factors that affect the selectivity and current density of the cathode are surface area, porosity, and conductivity. To catalyze the reaction at the anode, noble metals or their alloys such as a platinum/tungsten/nickel alloy can be used. Out of the three types of cells, direct glucose fuel cells have the advantage that they are the most robust and biocompatible.

1.5 Abiotic Fuel Cell Structure

Abiotic fuel cell can be implanted inside or on the surface of an organism where there is an abundance of glucose and oxygen. An organism's vascular system can act as the medium to conduct the reactants and help to remove the byproducts of the fuel cell reactions. The problem with this approach however is that glucose and oxygen exist as mixtures in body fluid. There is no catalyst currently known that selectively oxidizes glucose in the presence of oxygen. As such, a mixed potential is developed on the cell. To solve this problem, researchers have proposed the use of the stacked structure in which the cell is open to fluid only on one side. The stacked structure is shown in Figure 1.2.

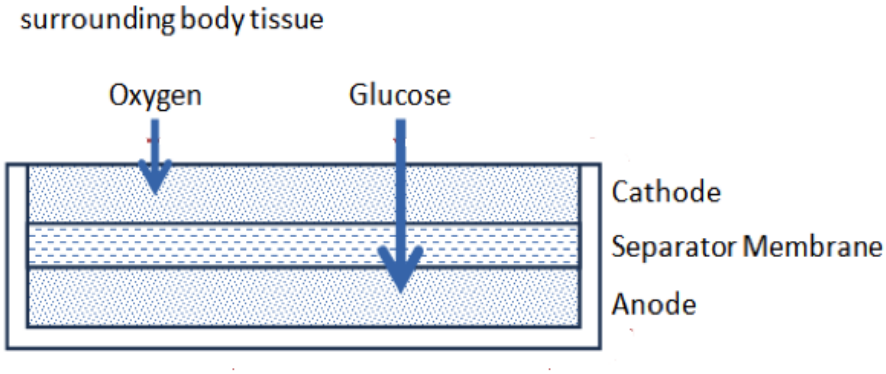

Figure 1.2 Stacked Structure for Glucose Fuel Cell

The porous cathode rests at the top and is exposed to the solution. The anode lies on an impermeable substrate at the bottom. Oxygen is reduced at the cathode before reaching the anode. As such, the concentration of oxygen at the anode should be low enough that the mixed potential is small.

There are several design considerations for such stacked glucose fuel cell structures. Firstly, an optimum inter-electrode distance exists. This is because as the distance between the electrodes increase, the concentration of oxygen at the anode is decreased, reducing the mixed potential effect and helping to increase the cell potential. However, as the inter-electrode distance increases, the glucose concentration at the anode also reduces, and therefore the potential of the cell tends to decrease.

For the fuel cell, a separation membrane can be present or absent. Removing the separation membrane helps to reduce the internal resistance of the cell. However, without a separating membrane, there is a risk that the electrodes will be shorted together. Such a separating membrane needs to be permeable to glucose and oxygen. Examples of such materials include dialysis or cellulose membranes soaked in poly-vinyl alcohol, or hydrophilic polyethersulfone membranes with 450 nm pores.

Lastly, a biocompatible structural support such as polycarbonate is necessary to reduce the inflammatory response that implanting such devices might cause. From the literature, abiotic fuel cells have been shown to generate between 2uW/cm^2 to 5uW/cm^2 [8,9,10]. Typically, at the beginning the fuel cell generates peak power. However, due to biological response to the implanted cell, the power would decrease over time through aging or fouling of the electrode or by diffusion resistance that is caused by tissues that form around the implant.

In this chapter, we have introduced some of the basic design considerations of the direct glucose fuel cell, one of which is the spacing between the two electrodes. In the next chapter, we will see how by modeling quantitatively various aspects of the direct glucose

fuel cell, we could gain a deeper understanding of how these dimensional tradeoffs arise for the direct glucose fuel cell.

2

Glucose Fuel Cell Theory and Modeling

Having introduced the basic operating and design principles of the glucose fuel cell in the previous chapter, in this chapter, we describe the theory and modeling aspects of direct glucose fuel cells in more detail in order to understand how to optimally design these cells. In particular, we formulate the form of the Current-Voltage characteristic of a typical fuel cell, taking into account major losses associated with the fuel cell operation including activation loss, concentration loss and Ohmic loss. In the second part of the chapter, we will describe a simple concentration model of the stacked glucose fuel cell, and based on this model, will provide some conclusions on the optimum dimensions of the glucose fuel cell.

2.1 Fuel Cell Theory and Voltage-Current Characteristics

As explained in Chapter 1, the overall reaction of a fuel cell is the exothermic oxidation of the fuel by oxygen. For example, the hydrogen fuel cell has the following overall reaction equation:

$$2H_2 + O_2 \rightarrow 2H_2O + \text{heat}$$

The amount of heat released in the reaction is called the enthalpy of the reaction ΔH, which can be calculated from the heat of formation of the reactants minus the products.

In a fuel cell, not all of the enthalpy can be converted to useful work such as electricity. The portion of the amount of useful work is called the Gibbs free energy of the reaction and is given by:

$$\Delta G = \Delta H - T\Delta S$$

where ΔS is the change in the entropy of the reaction.

The theoretical potential of a fuel cell can be calculated from the equation:

$$E_0 = -\frac{\Delta G}{nF}$$

where n is the number of electrons involved in the reaction and F is the Faraday constant (the total electric charge of 1 mol of electrons).

The actual voltage of the fuel cell is usually less than the theoretical value due to voltage losses in the cell. In fact, the voltage associated with a fuel cell is given by the following equation:

$$E_{cell} = E_0 - E_{activation,loss} - E_{concentration,loss} - E_{Ohmic,loss}$$

There are three major losses associated with a fuel cell, which dictate the shape of the IV curves: the activation loss, the concentration loss, and the Ohmic loss. The activation loss

is the voltage potential difference from equilibrium needed to start the electrochemical reaction. It is given by the Butler-Volmer equation:

$$E_{activation,loss} = \frac{RT}{a_c F}\log(\frac{I}{i_{0c}}) + \frac{RT}{a_a F}\log(\frac{I}{i_{0a}})$$

where a_c and a_a are the transfer coefficients and i_{0c} and i_{oa} are the exchange current densities for the cathode and anode respectively. The transfer coefficients a_c and a_a are theoretically between 0 and 1; for metallic electrodes they are ~0.5. The exchange current densities i_{0c} and i_{oa} are functions of the catalyst loading and specific surface area.

The concentration loss is the voltage loss associated with the changes in the concentration of the reactants when a reactant is rapidly consumed at the electrode. This voltage drop is given by Nernst's equation:

$$E_{concentration,loss} = -\frac{RT}{2F}\log(\frac{(C_{02,cathode})^{1/2} \times C_{glu,anode}}{C_{gluconic}})$$

The Ohmic loss is the loss associated with the internal resistance of the cell, which consists of the resistance to the flow of ions in the electrolyte, and the resistance to the electron flows in connecting wires. It is simply given by Ohm's law:

$$E_{Ohmic,loss} = I \times Rloss$$

Putting all three major losses together, we obtain the equation that describes the IV characteristic of the fuel cell:

$$E_{cell} = E_0 - \frac{RT}{a_c F}\log(\frac{I}{i_{0c}}) - \frac{RT}{a_a F}\log(\frac{I}{i_{0a}}) + \frac{RT}{2F}\log(\frac{(C_{02,cathode})^{1/2} \times C_{glu,anode}}{C_{gluconic}}) - I \times Rloss$$

A typical plot of the IV curve is shown in Figure 2.1.

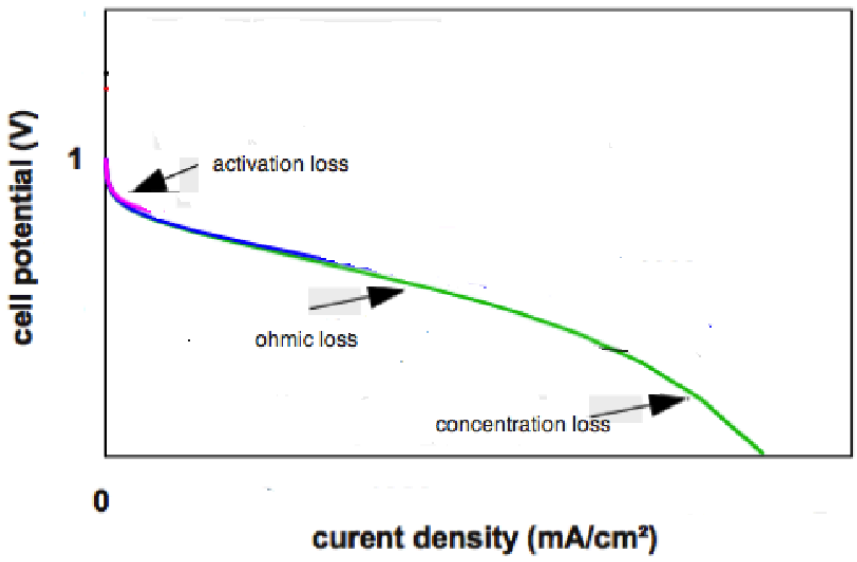

Figure 2.1 Typical Fuel Cell I-V Characteristic

There are three distinct regions where each of the major losses will dominate. When the current density is low, activation loss dominates. When the current density is high and the concentrations of reactants are reduced significantly, concentration loss dominates. For intermediate current density levels, the Ohmic loss dominates.

2.2 Abiotic Glucose Fuel Cell Concentration Model

A simple concentration model can be derived for the stacked structure of the abiotic glucose fuel cell. The diagram below illustrates the stack structure and the concentrations of glucose and oxygen in each respective region.

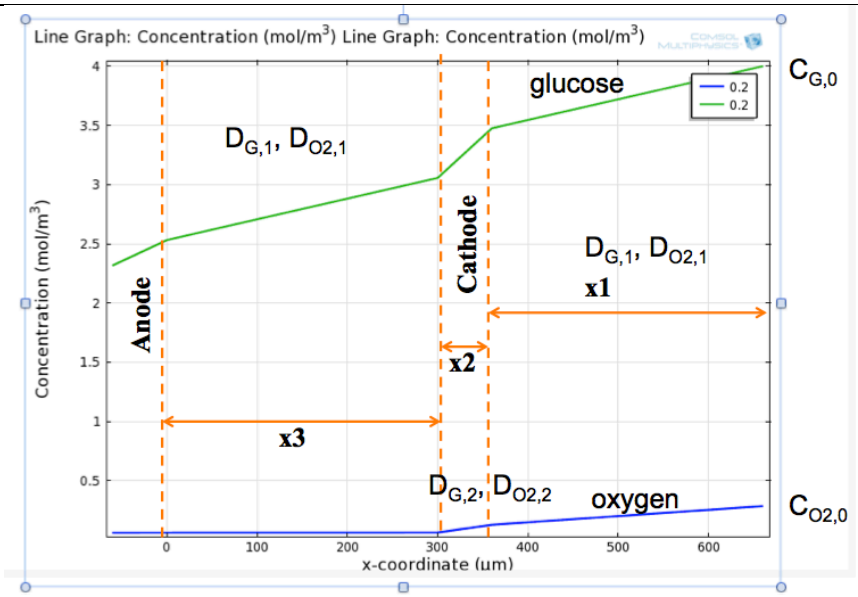

Figure 2.2 Concentration Profiles for Stacked Glucose Fuel Cell

In the solution far away from the cell (distance x1), the concentrations of glucose and oxygen are assumed to be constant and have the steady state values of $C_{G,0}$ and $C_{O2,0}$ respectively. x2 refers to the cathode thickness and x3 refers to the inter-electrode distance.

Let the flux densities for the main reaction and the mixed potential reaction be J and $J_{O2,p}$ respectively. These are related to the overall current through the fuel cell by

$I = 2qNA(J - J_{O2,p})$.

Fick's Law of Diffusion describes the relationship between the diffusion flux and the concentration gradient of the diffusive species:

$$J = -D\frac{\partial C}{\partial x},$$

where J is the diffusion flux, D is the diffusion coefficient, C is the concentration, and x is the dimension over which the diffusion occurs.

Using Fick's Law of Diffusion, the concentration of glucose at the anode is given by

$$C_{glu,anode} = C_{G,0} - (J + J_{O2,p}) \times (\frac{x1}{D_{G,1}} + \frac{x2}{D_{G,2}}) - J_{O2,p} \times (\frac{x3}{D_{G,1}})$$,

where $D_{G,1}$, $D_{G,2}$ refer to the diffusion coefficient in the solution and through the cathode respectively. As the expression shows, as the inter-electrode distance x3 becomes larger, the glucose concentration at the anode $C_{glu,anode}$ is reduced.

Similarly, the concentration of oxygen at the cathode is given by the expression

$$C_{O2,cathode} = C_{O2,0} - (J + J_{O2,p}) \times (\frac{x1}{D_{O2,1}} + \frac{x2}{D_{O2,2}})$$.

Assuming the reaction is oxygen-limited, the maximum flux density is approximately given by

$$J_{max} = \frac{C_{O2,0}}{x1/D_{02,1} + x2/D_{O2,2}}$$,

from which a deduction can be made that thinner cathode thickness is preferred for maximum current density of the fuel cell.

The concentration of gluconic acid at the anode is

$$C_{gluconic} = J \times (\frac{x1}{D_{G,1}} + \frac{x2}{D_{G,2}} + \frac{x3}{D_{G,1}})$$,

which implies that thinner dimension for the fuel cell will promote removal of byproducts of the reaction.

The concentration of oxygen at the anode is

$$C_{O2,anode} = C_{O2,0} - (J + J_{O2,p}) \times (\frac{x1}{D_{O2,1}} + \frac{x2}{D_{O2,2}}) - J_{O2,p} \times \frac{x3}{D_{O2,1}}$$.

The reaction kinetics for oxygen at the anode are given by

$$J_{O2,p} = K_{02} \times C_{O2,anode}$$.

$$J_{O2,p} = K_{02} \times (C_{O2,0} - (J + J_{O2,p}) \times (\frac{x1}{D_{O2,1}} + \frac{x2}{D_{O2,2}}) - J_{O2,p} \times \frac{x3}{D_{O2,1}})$$

.

Solving the above equation for $J_{O2,p}$, the flux density for the mixed potential reaction is:

$$J_{O2,p} = K_{02} \times (C_{O2,0} - J \times \frac{x1/D_{O2,1} + x2/D_{O2,2}}{1 + K_{O2} \times (x1/D_{O2,1} + x2/D_{O2,2} + x3/D_{O2,1})}$$

.

As we can see, the mixed potential reaction $J_{O2,p}$ is smaller if the inter-electrode distance x3 increases.

Taking into account the mixed potential current, the IV characteristic of the cell becomes

$$E_{cell} = E_0 - \frac{RT}{a_c F}\log(\frac{I + 2qNAJ_{O2,p}}{i_{0c}}) - \frac{RT}{a_a F}\log(\frac{I + 2qNAJ_{O2,p}}{i_{0a}}) + \frac{RT}{2F}\log(\frac{(C_{02,cathode})^{1/2} \times C_{glu,anode}}{C_{gluconic}}) - I \times Rloss$$

$$E_{cell} = E_0 - \frac{RT}{a_c F}\log(\frac{I + 2qNAJ_{O2,p}}{i_{0c}}) - \frac{RT}{a_a F}\log(\frac{I + 2qNAJ_{O2,p}}{i_{0a}}) + \frac{RT}{2F}\log(C_{glu,anode}) + \frac{RT}{2F}\log(\frac{(C_{02,cathode})^{1/2}}{C_{gluconic}}) - I \times Rloss$$

The output power of the cell is thus

$$P = I\{E_0 - \frac{RT}{a_c F}\log(\frac{I + 2qNAJ_{O2,p}}{i_{0c}}) - \frac{RT}{a_a F}\log(\frac{I + 2qNAJ_{O2,p}}{i_{0a}}) + \frac{RT}{2F}\log(C_{glu,anode}) + \frac{RT}{2F}\log(\frac{(C_{02,cathode})^{1/2}}{C_{gluconic}}) - I \times Rloss\}$$

From the previous discussion, as the inter-electrode distance x3 increases, both $J_{O2,p}$ and $C_{glu,anode}$ are reduced. Since the effect of these terms are opposite in the overall power equation, one can see that there may be an optimum inter-electrode distance for maximum power density.

For illustration, we implemented the model in Matlab with an example set of parameters. A plot for the current-voltage characteristics and the power density are shown below.

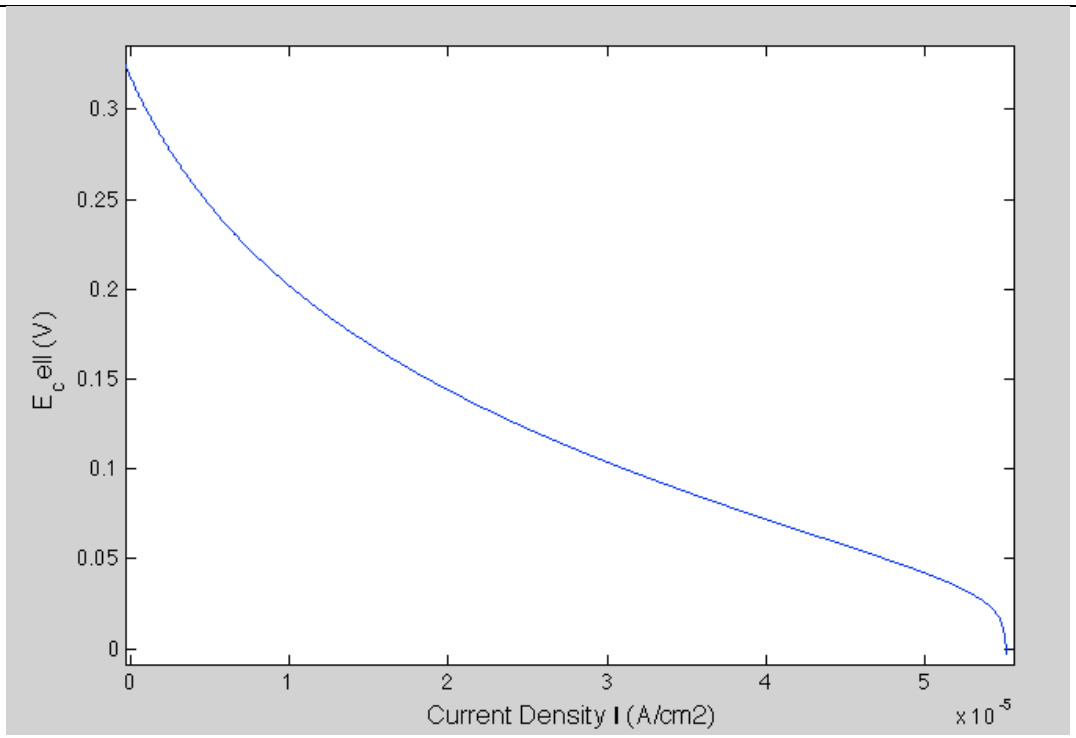

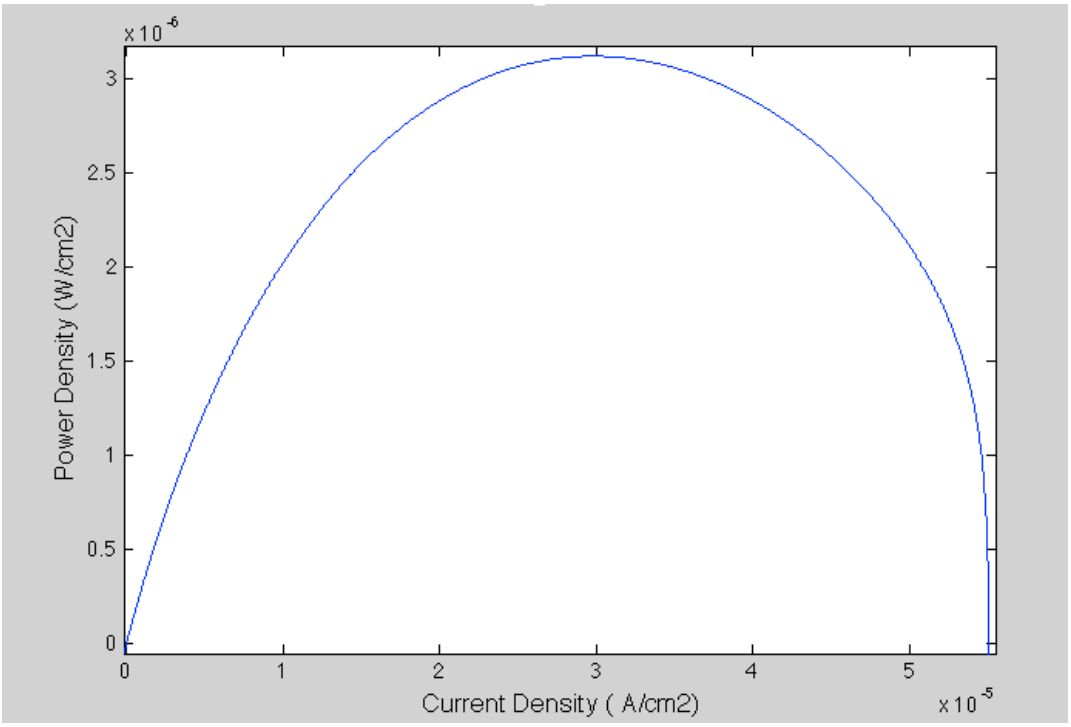

Figure 2.3 Matlab-derived Current Voltage and Power Density Curves

A sweep of maximum power density versus the inter-electrode distance x3 is performed and the result is shown in the figure below

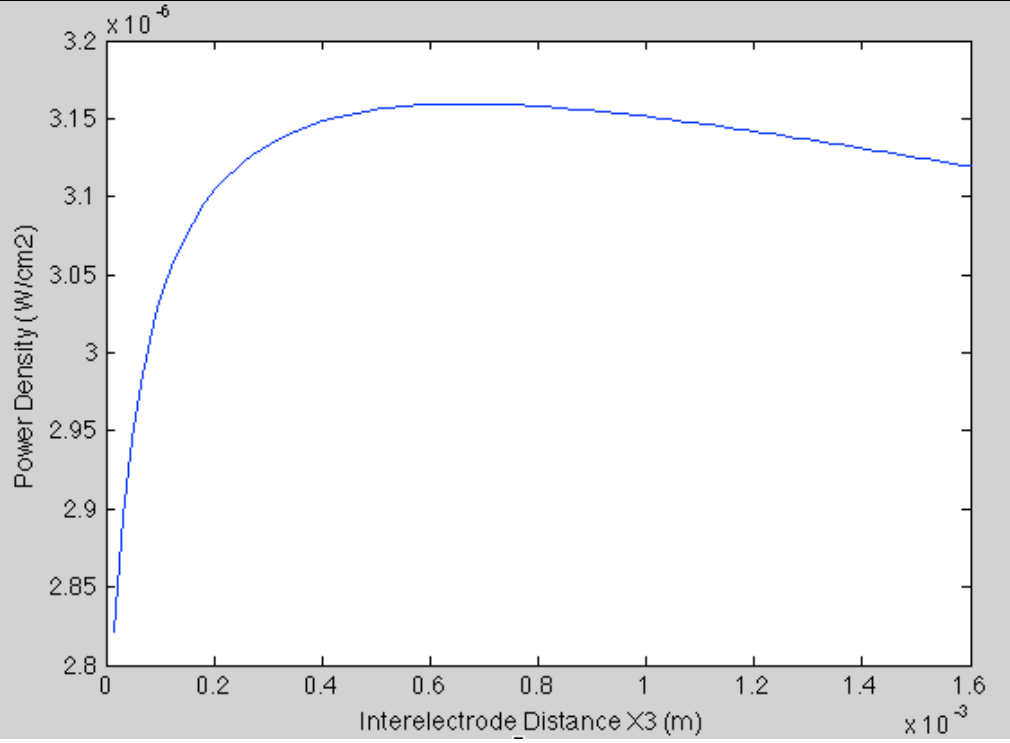

Figure 2.4 Matlab-derived Plot of Maximum Power Density vs x3

As we can see, there is an optimum distance for x3, which could be determined experimentally. Usually this optimal inter-electrode distance is very small, in the order of a few hundreds of micrometers. In the next chapter, we will see how our proposed fabrication and assembly method could bring down the size of the fuel cell significantly, allowing such small inter-electrode distance to be obtained.

3

Glucose Fuel Cell Fabrication and Assembly

In the previous chapter, we have shown how to theoretically model the direct glucose fuel cell to determine the form of the Current-Voltage characteristics and to attain key optimal, usually small, dimensions for the glucose fuel cell. This chapter touches on the more practical aspect of how to fabricate and assemble the direct glucose fuel cell in such a way that this miniaturization can be achieved. In particular, section 3.1 describes the major issues and challenges of the electrode fabrication and assembly steps, which are elaborated upon in section 3.2 and 3.3 respectively.

3.1 Fabrication and Assembly Issues and Challenges

Our challenge is to develop a fuel cell structure that is amenable to miniaturization and is easy to assemble. This is achieved with a construction technique that uses only a one-piece casing instead of methods that use two parts requiring fastening. This assembly technique is described in section 3.3. The cathode needs to be porous to allow the diffusion of glucose into the cell. In addition, the cathode needs to have high surface area for catalytic activity. For these reasons, we choose to use Pt on carbon paper as our cathode. For the anode, a catalyst with high surface area that has high reactivity with glucose is needed. To satisfy this requirement, we select Raney-type Pt/Ni alloy as our anode. The Raney-type Pt/Ni alloy has been found to have higher catalytic activity than Pt black [9]; the electrode fabrication is described in detail next. We follow the fabrication process steps as described in [8].

3.2 Electrode Fabrication

The cathode is fabricated by sputtering a 100nm layer of Pt onto both sides of a porous carbon paper. 20nm of Ti is used as the adhesion layer to promote adhesion. Sputtering is chosen as the preferred method over electron-beam evaporation due to the higher quality of the Pt adhesion achieved.

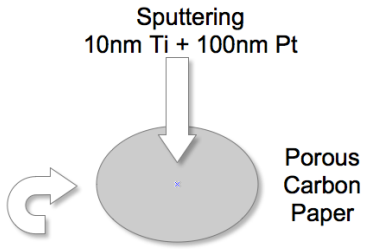

3.1(a)

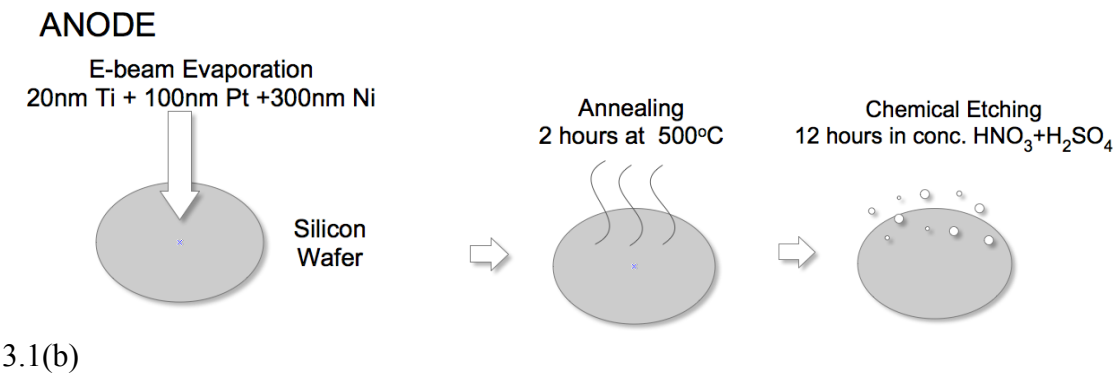

3.1(b)

Figure 3.1 Fabrication Steps (a) Cathode (b) Anode

For the anode, E-beam evaporation is used to deposit 20nm of Ti, 100nm of Pt, and 300nm of Ni in sequence onto a silicon wafer. The metals are then allowed to anneal by heating for 2 hours at 500^0C in an oxygen-free nitrogen environment. The absence of oxygen is important to prevent an oxide layer from being formed. The two metals will alloy by diffusion to form a Pt/Ni alloy. Next, the unalloyed Ni is removed by chemical etching for 12 hours in a 1:1 mixture of concentrated nitric acid and sulfuric acid. This process produces Raney-type Pt/Ni that has high surface area as shown in the following photograph.

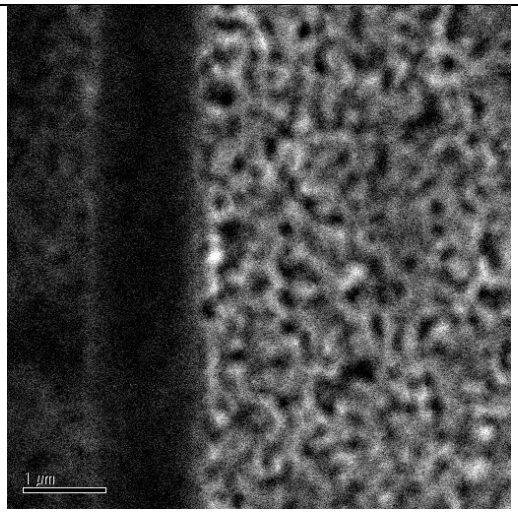

Figure 3.2 SEM Micrograph of a fabricated anode.

The cathodes and anodes are subsequently diced into the desired dimensions and cleaned via cyclic voltammetry in de-aerated 0.5M H_2SO_4. It is important to use de-aerated solution to prevent oxidation from occurring. For the cathode, cyclic voltammetry is performed through 20 cyclic sweeps in steps of 50mV/s between 1.3V and -0.3V versus a glass Ag/AgCl reference electrode. For the anode, 10 cyclic voltammetry sweeps in steps of 10mV/s between 1.3V and -0.3V are performed.

3.3 Fuel Cell Assembly

After cleaning, the electrodes are then inserted into the holder as shown in the following diagram.

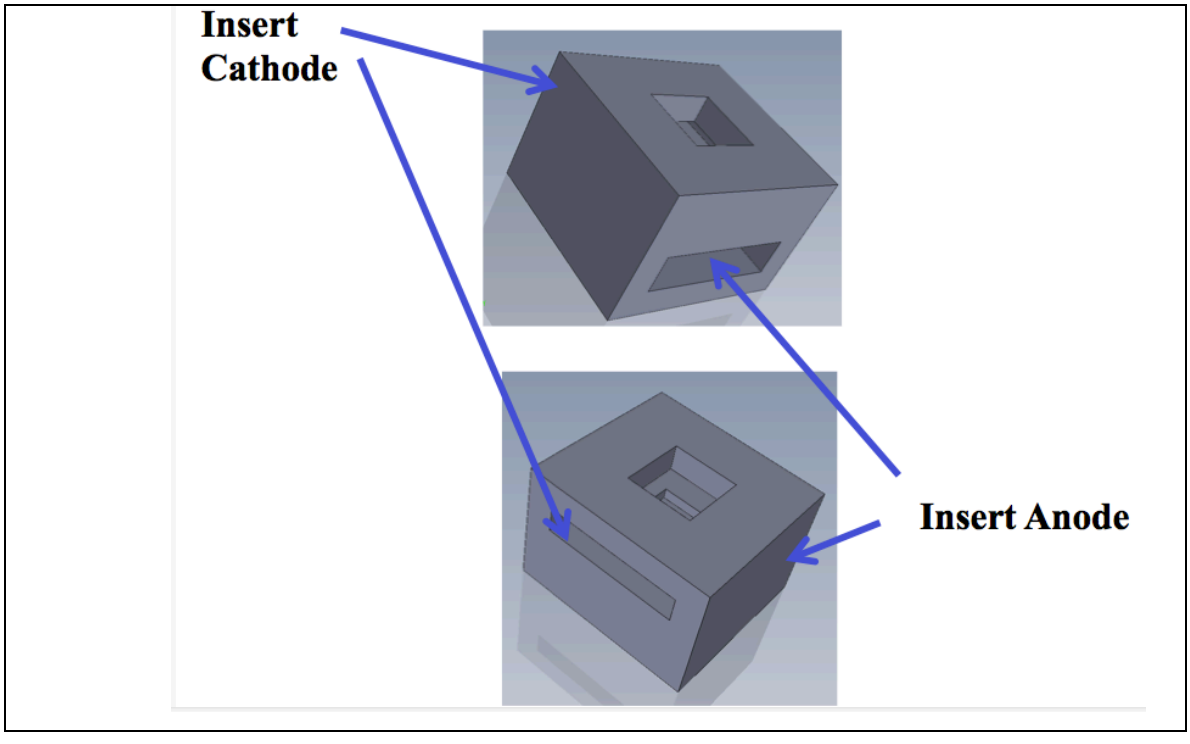

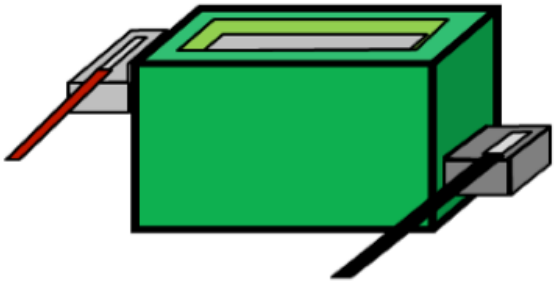

Figure 3.3 Fuel Cell Assembly

The holder is micro-fabricated via 3-D printing using polycarbonate as the material. It has two slots on the sides for the electrodes and an opening at the top for the diffusion of glucose and oxygen. The one-piece holder allows cell to be easily shrunk to 1mm x 1mm. For lower internal resistance and ease of assembly, we do not use a separating membrane. Copper wires were connected to the electrodes with silver epoxy or through soldering on the two sides. The entire structure is sealed with hot glue, leaving only the top opening exposed to the solution. It is important to seal the cell from the solution to prevent the false potential resulting from dissimilar metals from interfering with the observed results. Care also has to be taken to prevent trapped oxygen in the gap between the two electrodes. Figure 3.4a shows a size comparison between the $1mm^2$ cell and a penny. Figure 3.4b shows a completely assembled and sealed cell.

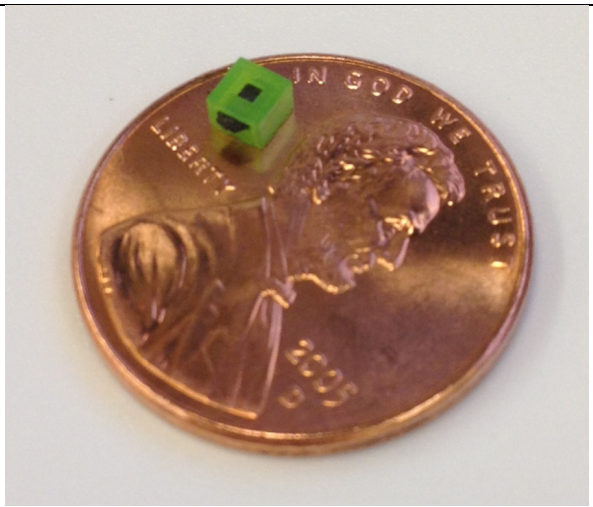

Figure 3.4 Complete Fuel Cell (a)

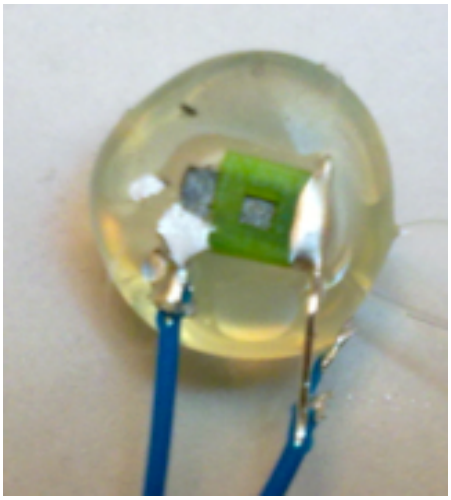

(b)

In the next chapter we will see how the miniaturized direct glucose fuel cells fabricated and assembled by the method described in this chapter could be tested and what their power performance and longevity are.

4

Experiments and Results

In the previous chapter, we have shown how to fabricate and assemble the direct glucose fuel cell to achieve miniaturization and low-cost prototyping. This chapter describes the series of experiments we performed on such fabricated fuel cells. First, we report the results for the half-cell voltage experiments, which confirm the functionality of our electrodes and the viability of the stacked structure in the ideal case. Next, we report the experimental results and the power density performance of the fuel cells in an actual enclosed structure. In addition, we perform an experiment to determine the longevity of our fuel cell. Finally, we suggest some methods for improvement.

4.1 Half-Cell Voltage Experiments

(a) Experimental Procedures:

We first performed a half-cell experiment to ensure that our electrodes function as expected in an ideal environment. The set-up depicted in Figure 4.1 was constructed. This setup consisted of two half-cells: the anode chamber and the cathode chamber, connected through a salt bridge.

The salt bridge was made by boiling KCl and agar 5% solution together and pouring the resulting hot mixture into a glass tube, where it would solidify. The salt bridge allows the free exchange of proton and hydroxide ions between the chambers.

A 5mM glucose solution was prepared in each chamber by mixing 0.09 gram of anhydrous glucose and 100mL of 0.01M phosphate buffered saline solution.

Each $1cm^2$ piece of anode and cathode was made and attached to a properly sealed copper wire. The cathode and anode were fully submerged in their respective chambers. Oxygen was removed from the anode chamber by continuously supplying Nitrogen into the enclosed chamber. The purpose of this is to prevent a mixed potential from forming by reducing the concentration of dissolved oxygen in the anode chamber to very low levels. The cathode chamber is exposed to air at atmospheric pressure.

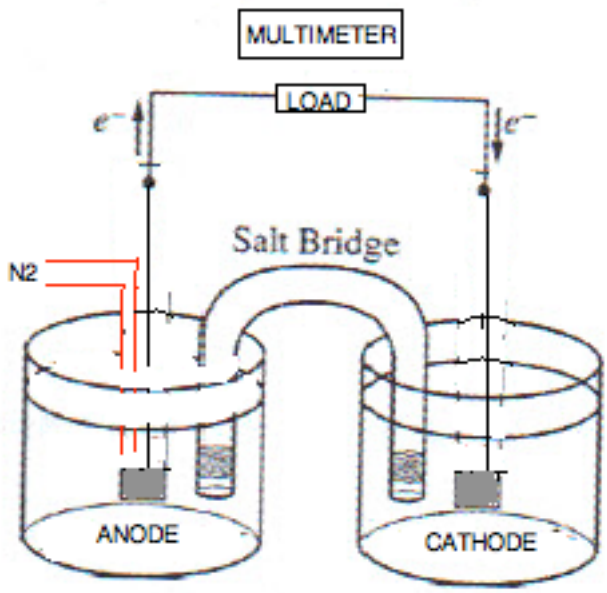

Figure 4.1 Half Cell Set-up with Salt Bridge. Adapted from [12]

(b) Results:

The set-up was allowed to stabilize for approximately 24 hours and an I-V characterization of the cell was performed by sweeping the load resistance values between 1MOhm and 1kOhm with a 10 minute settling time interval between measurements. The following graph shows the IV curve obtained and the calculated fuel cell power density versus current density.

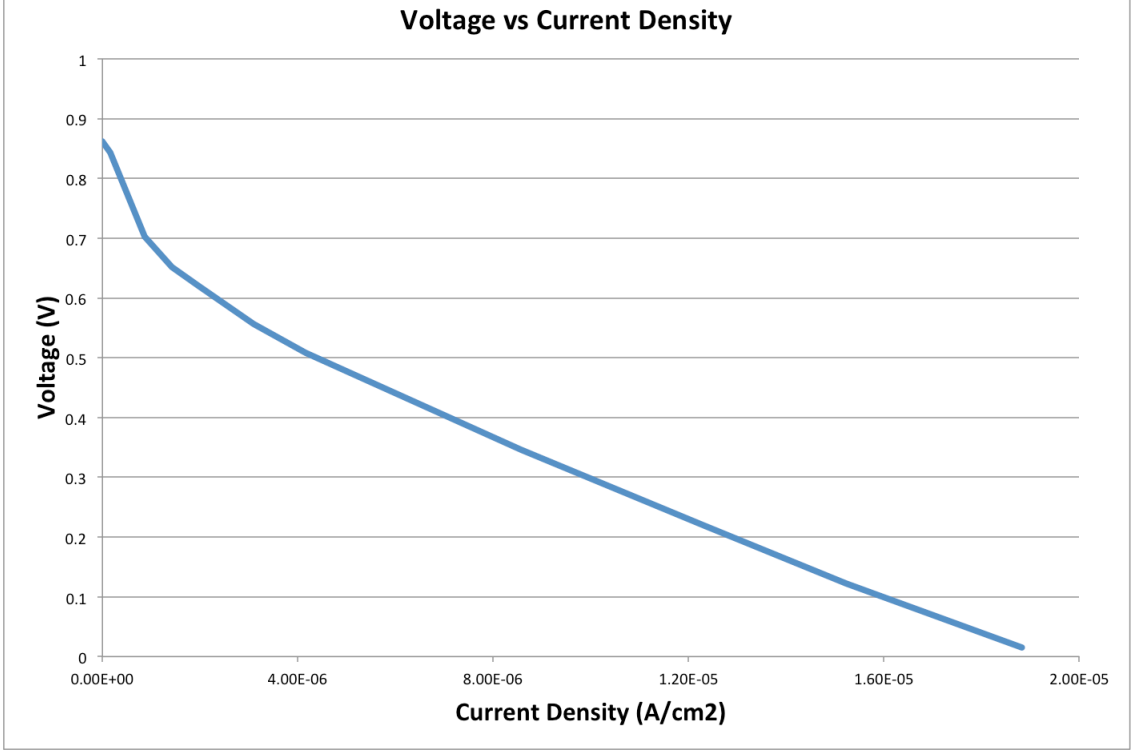

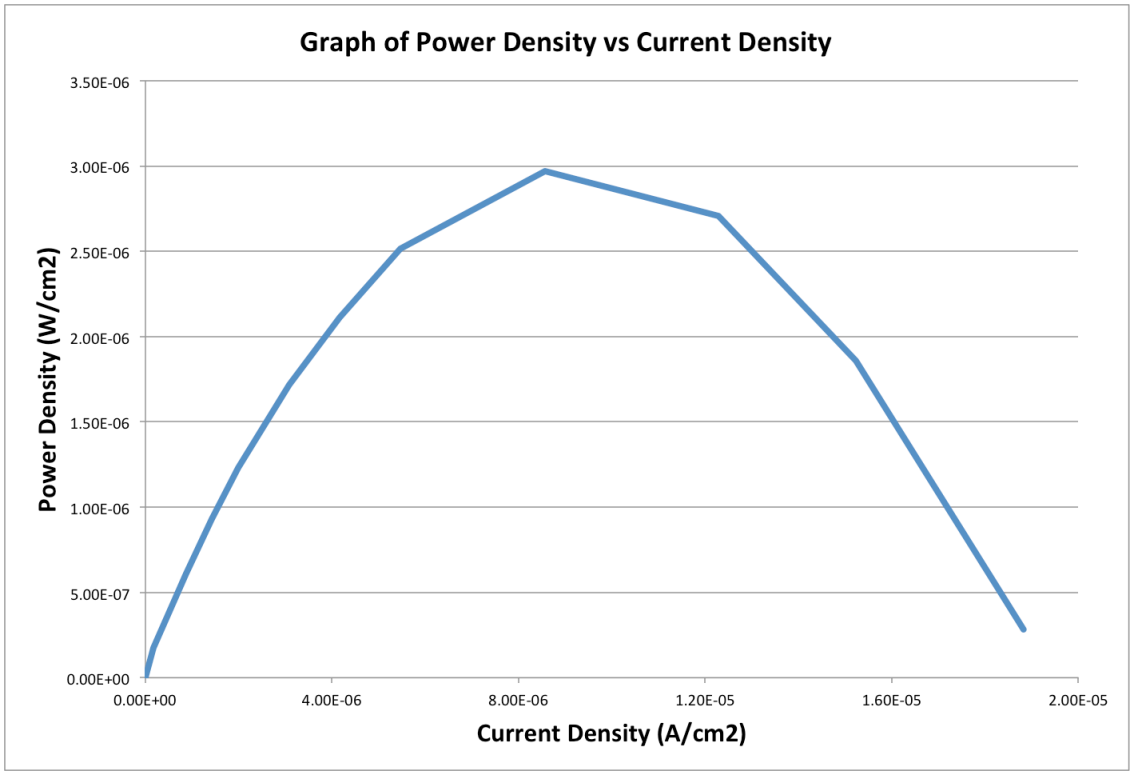

4.2(b)

Figure 4.2 (a) top: IV curve (b) bottom: Power density curve

As shown, the open-circuit voltage of the cell is about 0.9V. The cell achieved a maximum power density of 3uW/cm^2 at a current density of around 10uA/cm^2. The maximum current density is about 20uA/cm^2.

4.2 Fuel Cell Closed Structure Experiments:

(a) Experimental Procedures:

The 1mm^2 fuel cell was constructed based on the procedures described in Chapter 3, and the resulting cell was tested with the following set-up.

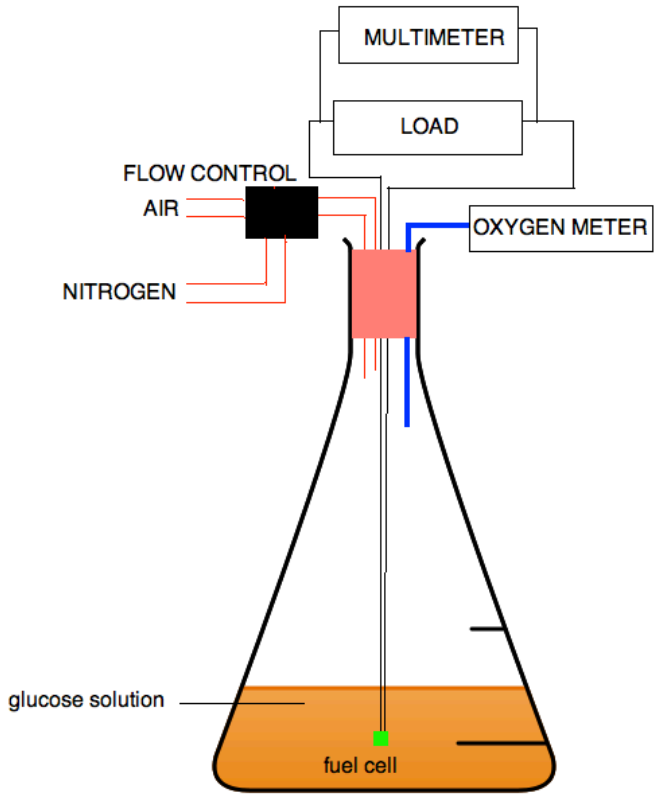

Figure 4.3 Fuel Cell Experiment Setup

Similar to the previous experiment, a 5mM glucose solution was prepared by mixing 0.09 grams of anhydrous glucose into 100mL of 0.01M phosphate buffered saline solution in a conical flask. The fuel cell was introduced into the flask and fully submerged in the solution. The cell potential was measured with a Keithley 2612 SourceMeter/Multimeter controlled by a computer running MATLAB. The load resistance sweep was performed with an analog multiplexer chip ADG726 controlled via an FPGA XEM3001 with a 10 minute settling time interval between each measurement. The load resistance ranges from 8MΩ to 100kΩ. The flask was sealed off with a plug and adhesive materials. The oxygen concentration inside the flask was varied by controlling the relative flow rate of input nitrogen and air mixture. The internal oxygen concentration was monitored with an OxyMicro oxygen meter. For this experiment, the oxygen concentration was controlled at 10%.

(b) Settling time experiment:

We first performed an experiment to determine whether the waiting time of 10 minutes is adequate for the fuel cell voltage to settle down between changing the load resistance values. Figure 4.6 shows the voltage of the cell when its current sink is changed at 5min intervals starting at time t = 10 mins. The voltage plot shows that the cell voltage settles after roughly 5 mins.

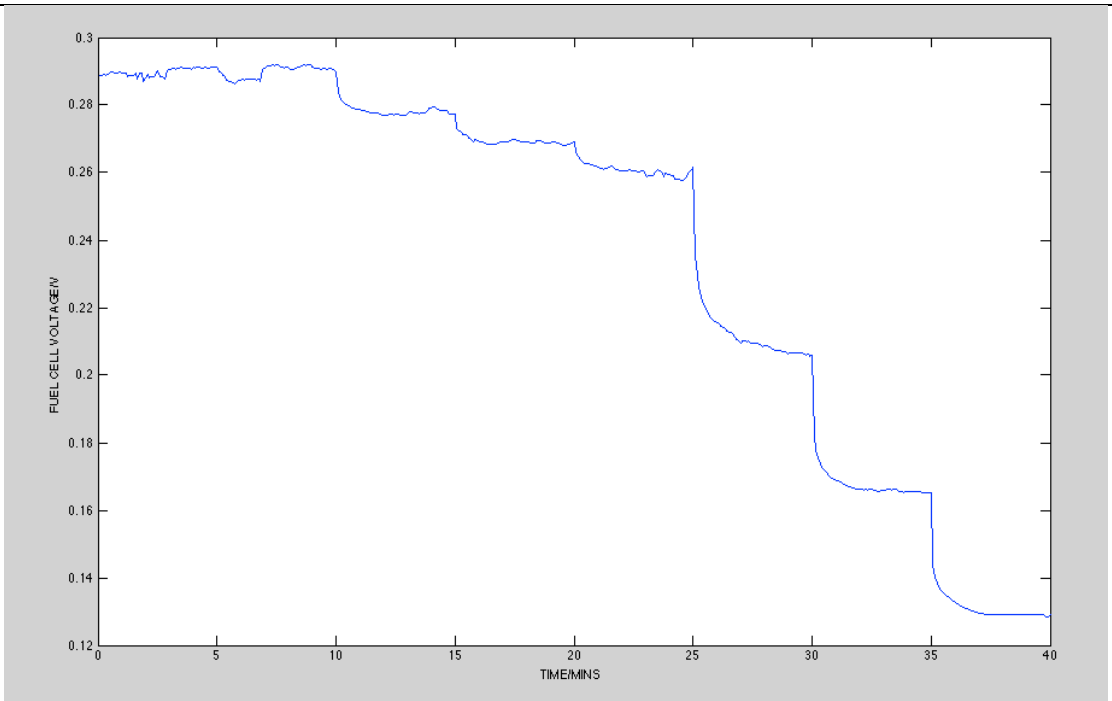

Figure 4.4 Settling Time

(c) Results:

Next, the power of the fuel cell was measured by recording the fuel cell voltage while sweeping the load resistances for different values between 8MΩ and 100kΩ with 10 minute intervals. The following graph shows the obtained initial IV curve and power density curves.

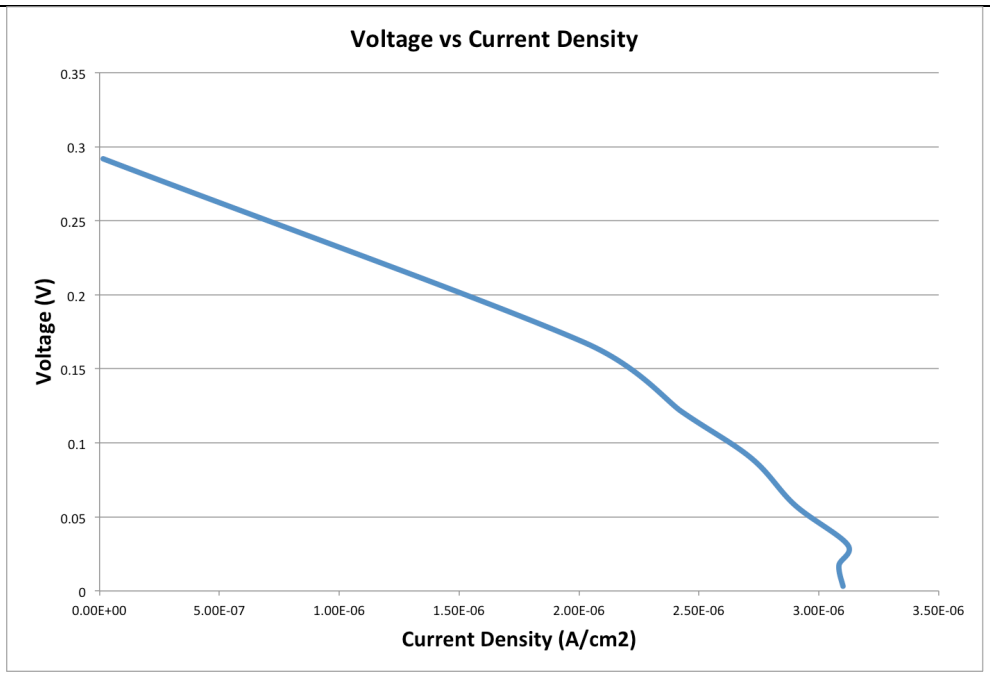

4.3 (a)

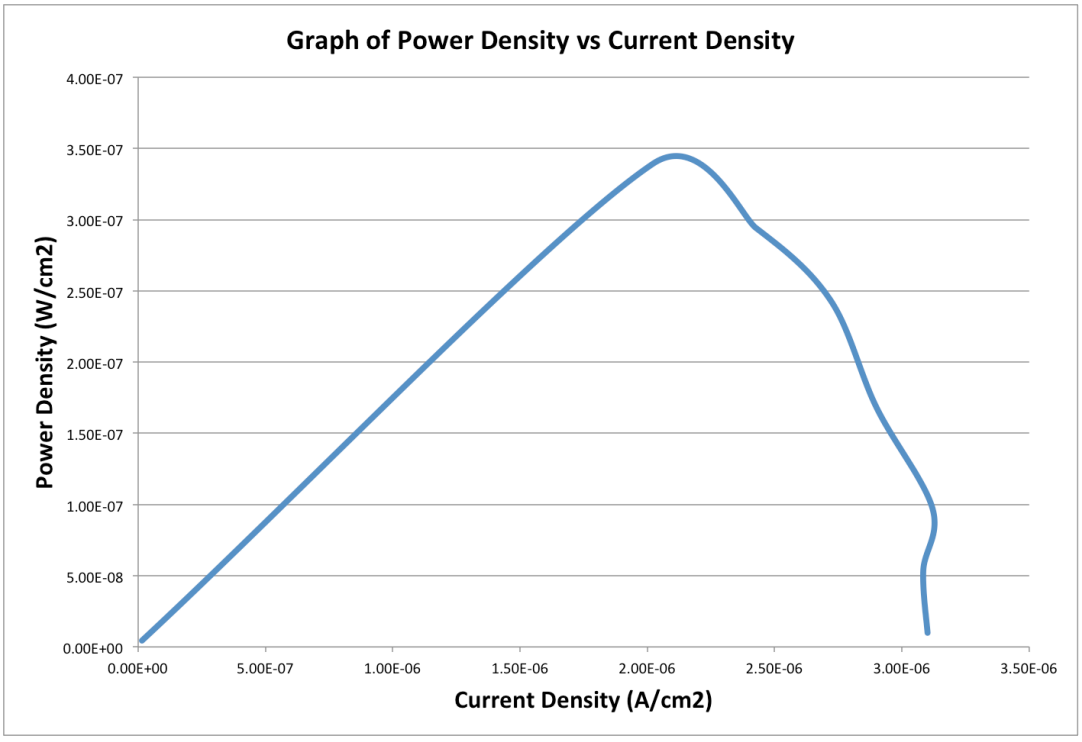

4.3 (b)

Figure 4.5 (a) IV curve (b) Power density curve

As we can see, the open circuit potential is about 300mV, and the maximum power density is about 0.34uW/cm^2 for a current density of 2uA/cm^2. The maximum current density that can be obtained is around 3.1uA/cm^2. The lower power density of the fuel cell compared to the half-cell experiment may be attributed to the incomplete removal of the oxygen at the anode, leading to mixed cell potential.

(d) Degradation measurements:

The power density was continuously measured for the cell and the resulting power density curves are plotted on the same axis in Figure 4.4. The waiting time between each power curve is 4 hours 20 minutes, for a total of 39 hours measurement time (9 power curves). The power density decreases from 0.34uW/cm^2 to 0.008uW/cm^2 in 39 hours.

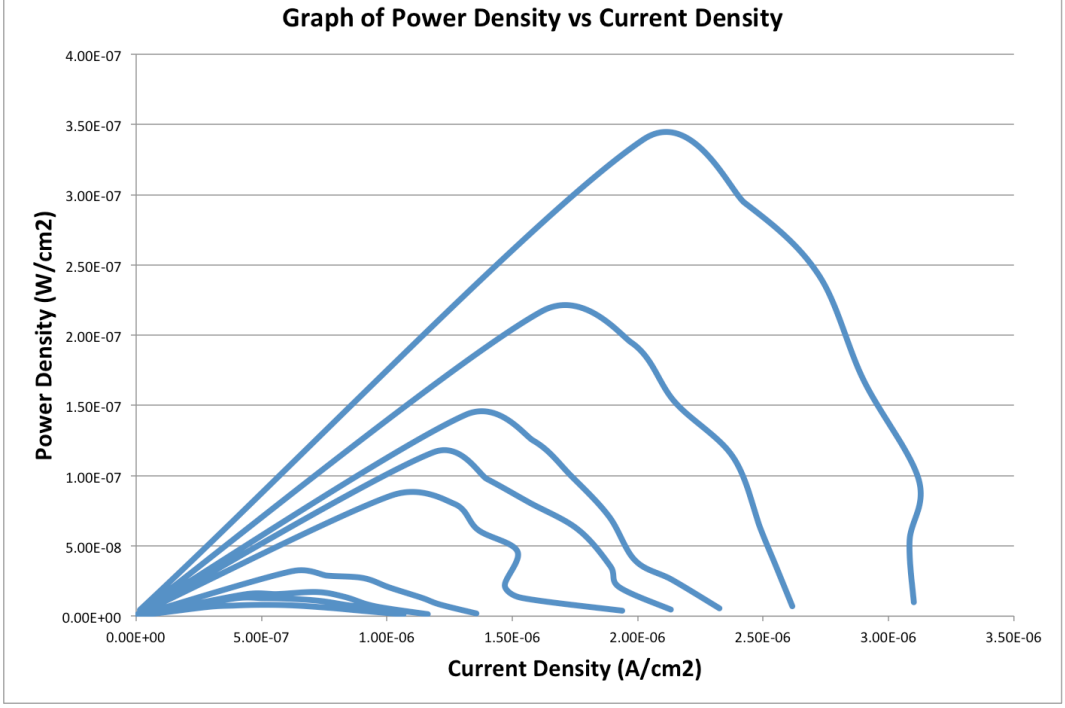

Figure 4.6 Power Density Degradation

The following graph shows the decay of the maximum power density versus time.

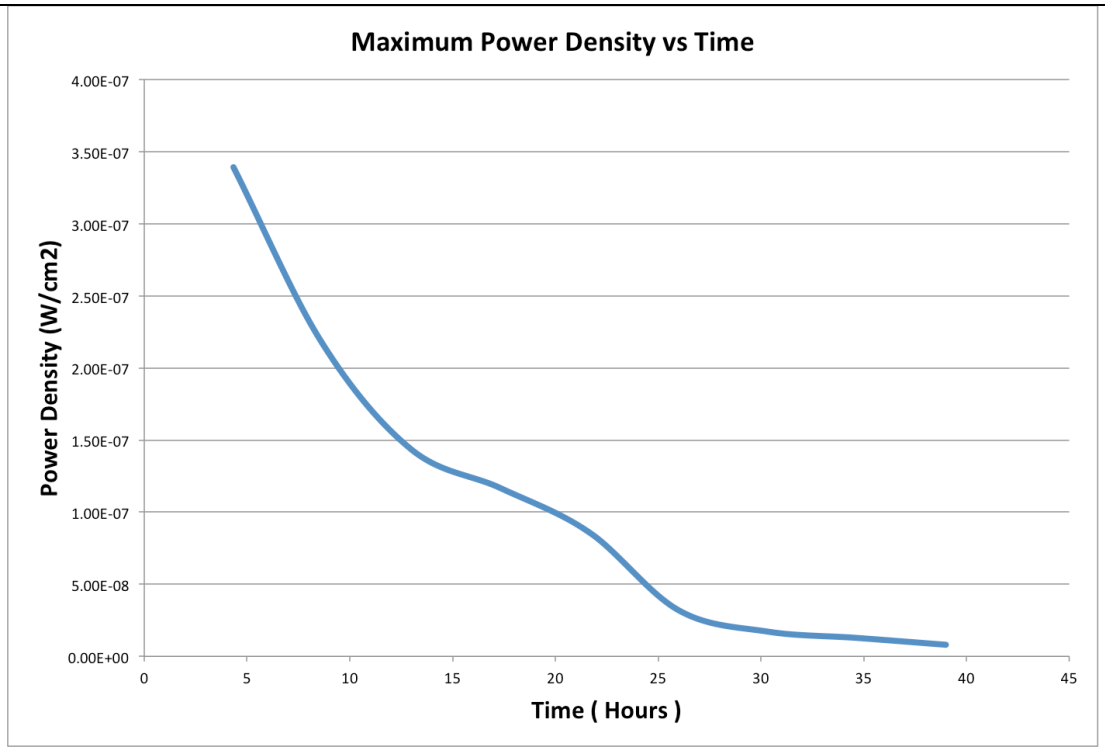

Figure 4.7 Power Density vs Time

From the plot, the half-life of the fuel cell power density decay is about 10 hours.

4.3 Conclusion:

In this chapter, we have demonstrated that an ideal fuel cell with maximum reduction of oxygen at the anode can have an open voltage potential of 900mV and produce a maximum power density of up to 3uW/cm^2. An actual closed 1mm^2 structure, however, can only yield a maximum power density of 0.34uW/cm^2 and an open-circuit voltage of 300mV, possibly because of mixed potential due to the presence of oxygen at the fuel cell anode. In future studies, the use of a stronger catalyst towards oxygen reduction at the cathode might reduce the mixed potential effect. One option for such a material would be single-walled carbon nanotubes [10]. Single-walled carbon nanotubes provide a very high catalytic surface area while remaining porous to glucose. A better sealant than silicone hot glue could also be used to reduce the possibility of oxygen diffusing from the solution to the anode.

Although the power densities obtained for our miniaturized fuel cells are small, they could be used for low power applications that don't consume a lot of power. In the next chapter, we will describe one such application in touch body interface.

5

Example Application and Design Considerations

In the previous chapter, we have demonstrated the performance of our miniaturized direct glucose fuel cell. Having a power density of 0.34uW/cm^2, the possible application areas for such a fuel cell must be extremely low power in nature. An example of such an application for the glucose fuel cell is in powering wireless body interfaces on the skin, which will be discussed in this chapter.

5.1 Glucose Fuel Cell for Wireless Skin Implant

In the future, people will be able to use miniature body-interface implanted devices to communicate with personal devices such as smart-phones or with ambient computers to interact with their environment. In order to power such implanted devices, a conventional

solution based on batteries is impractical due to the limitation in implantation volume and lifetime requirements. To solve this problem, methods to generate power based purely on the permanent contact of the devices with the user's body are required. In this application, the glucose fuel cell can be implanted in the skin and harvest energy from glucose in the body that diffuses to the skin. The extracted energy could be used to power an electronic system performing some useful function. Figure 5.1 shows such a system. The system consists of a pressure sensor to detect user control input, a basic wireless communication to transfer the user input to an external base-station (such as a smart-phone), and a 1-pixel display as an indicator device.

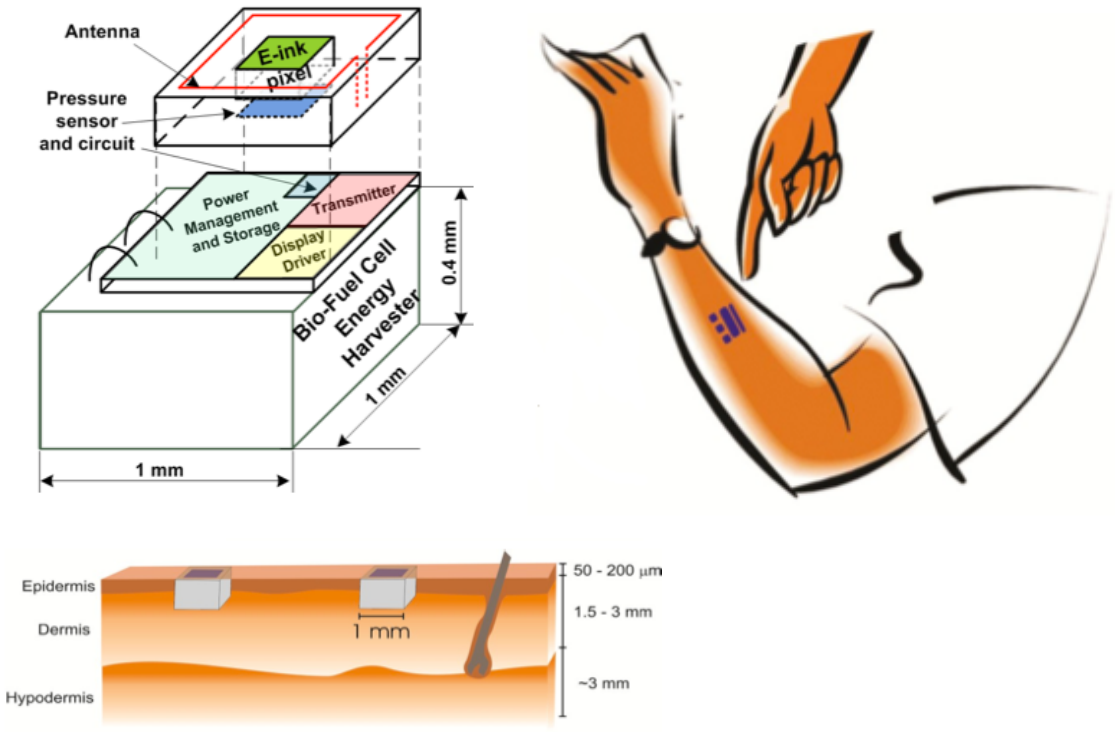

Figure 5.1 1mm3 Implantable communication and display systems powered by bio-fuel cells. Figure from [13]

A basic wireless communication system for this application would likely consist of a class-D switching power amplifier and an antenna. When the touch sensor is pressed, the power amplifier is turned on to drive the antenna. The efficiency of the power amplifier in driving the antenna is important in the design of such system as it determines the Signal to Noise Ratio of the system. In section 5.2 we will hence discuss design considerations to optimize the efficiency of the power amplifier.

5.2 Power Amplifier Design Considerations

Figure 5.2 shows a simplified power amplifier circuit with switch resistance R_s and input capacitance C_g driving an antenna with radiation resistance R_{rad}. The goal is to optimize the efficiency of the PA in delivering power to the antenna through the load R_{rad}.

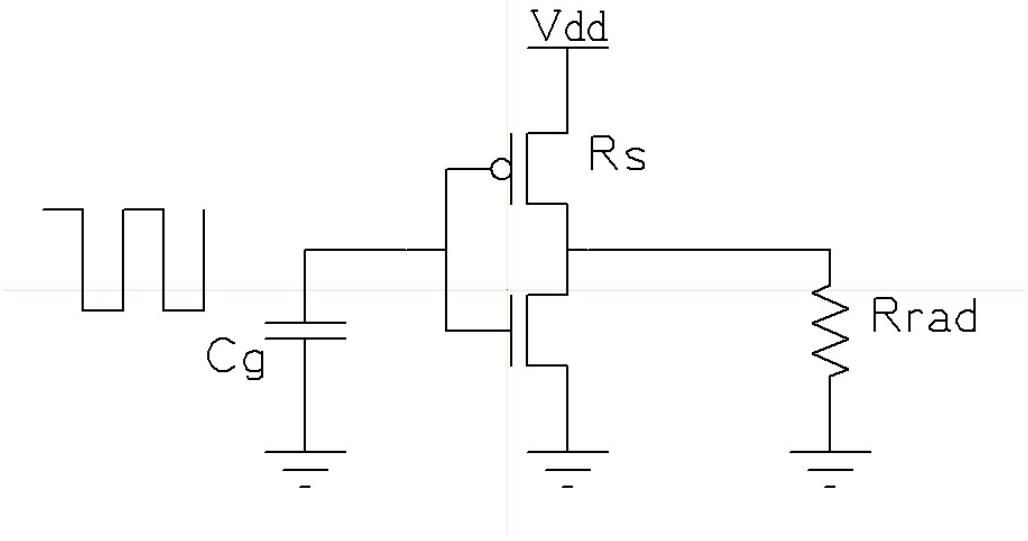

Figure 5.2 Simplified Power Amplifier Circuit and Antenna

Two variables to consider in the design of the power amplifier are the width of transistor in the power amplifier and the frequency of operation.

The resistance and gate capacitance of the switch are related to the device width through

$$R_S = \frac{R_{SW}}{W}$$

$$C_g = C_{gate} \times W$$

where R_{sw} and C_{gate} are process parameters.

For small electric dipole type antennas, the radiation resistance is given by the following expression (as given in [14]):

$$R_{rad} = \frac{R}{6\pi}\left(\frac{b}{l}\right)^2$$

where $l = \lambda/2\pi$, $R = 120\pi$ (the wave resistance in free space), b = height of cylindrical volume.

Thus the relation between the radiation resistance and frequency is given by

$$R_{rad} = R_k \times f_{osc}^2$$

where R_k is a constant of proportionality = $\frac{2\pi R}{3}\left(\frac{b}{c}\right)^2$, c is the speed of light.

The power delivered to the load is

$$P_L = \frac{1}{2} \times V_{SW}^2 / R_{rad} = \frac{1}{2} \times V_{dd}^2 \times R_{rad} / (R_{rad} + R_s)^2$$

The total power drawn from the power supply is

$$P_{VDD} = \frac{1}{2} \times V_{dd}^2 / (R_{rad} + R_S) + C_g \times V_{dd}^2 \times f_{osc}$$

Hence, the PA efficiency is

$$\eta = \frac{P_L}{P_{VDD}} = \frac{R_{rad}}{R_{rad} + R_S + 2 \times C_g \times f_{osc} \times (R_{rad} + R_S)^2}$$

$$\eta = \frac{1}{(1 + R_S/R_{rad})(1 + 2\times C_g \times f_{osc} \times (R_{rad} + R_S))}$$

To maximize the efficiency, we want to minimize

$$A = (1 + R_S/R_{rad})(1 + 2\times C_g \times f_{osc} \times (R_{rad} + R_S))$$

First, let's consider the simplest case where the frequency has been chosen and we want to maximize the efficiency of the power amplifier by optimizing the width of the power transistor.

For this case, the optimal width is given by[1]

$$W = \sqrt{\frac{R_{SW} \times \left(1 + 2\times C_{gate} \times f_{osc} \times R_{SW}\right)}{2\times C_{gate} \times f_{osc} \times R_{rad}^2}}$$

If the antenna is of the small electric dipole variant, the complete expression for W is

$$W = \sqrt{\frac{R_{SW} \times \left(1 + 2\times C_{gate} \times f_{osc} \times R_{SW}\right)}{2\times C_{gate} \times f_{osc}^5 \times R_k^2}}$$

For the second case, we assume that the frequency has not been chosen and is also one of the optimization variables. We now also take into consideration the antenna loss resistance R_{ant} which is the Ohmic loss due to the resistance of the metal that constitute the antenna and the connections. The expression for A then becomes:

$$A = 1 + 2\times C_g \times f_{osc} \times (R_{rad} + R_{ant} + \frac{R_{SW}}{W}) + \frac{R_{ant} + \frac{R_{SW}}{W}}{R_{rad}} + 2\times \frac{R_{ant} + \frac{R_{SW}}{W}}{R_{rad}} \times C_g \times f_{osc} \times$$

$$(R_{rad} + R_{ant} + \frac{R_{SW}}{W})$$

Optimizing A with regard to the width, we obtain[1]

[1] The full derivation is available in Appendix 7.3

$$A \geq A(x) = \left(1 + \frac{R_{ant} \cdot 4 \cdot {C_{gate}}^2 \cdot {R_{SW}}^2}{R_k \cdot x^2}\right)\left\{1 + 2x + 2\sqrt{x + x^2}\right\}$$

$$= \left(1 + \frac{m}{x^2}\right)\left\{1 + 2x + 2\sqrt{x + x^2}\right\}$$

where m is a constant $= \frac{R_{ant} \cdot 4 \cdot {C_{gate}}^2 \cdot {R_{SW}}^2}{R_k}$ and x = $2 \times C_{gate} \times f_{osc} \times R_{SW}$. This expression can then be minimized numerically to obtain the optimum value for x, which corresponds to an optimum value for f_{osc}.

From the expression, we can see that if $R_{ant} = 0$, to minimize A, since x is positive $x \to 0$ or $f_{osc} \to 0$. However, for $R_{ant} \neq 0$, the solution to the optimization is a non-zero f_{osc}, which we will now illustrate with an example.

Numerical example:

As an example, we can assume that C_{gate} = 2fF/μm, R_{sw} = 1kΩ.μm, R_{ant} = 1Ω, and that the height of antenna cylindrical volume b = 1mm which leads to R_k = 8.7730e-21

Thus $m = \frac{R_{ant} \cdot 4 \cdot {C_{gate}}^2 \cdot {R_{SW}}^2}{R_k} = 0.0018238$

Plotting the expression A(x) with respect to x, we obtain the following figure

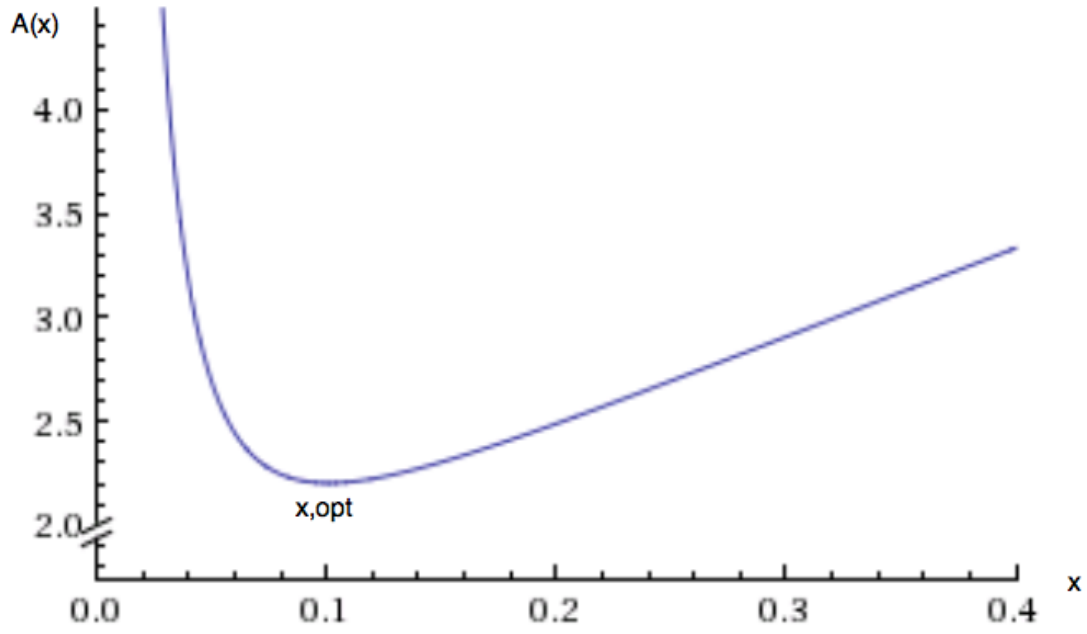

Figure 5.3 Plot of A(x) versus x

From the plot, we find that the minimum value for A(x) is 2.2 which happens at x = 0.101072. Thus the optimum frequency of operation happens at

$f_{osc} = x/(2\times C_{gate}\times R_{SW}) \; = \; 456MHz$

From the form of the expression for A(x), it could be noted that a larger value for R_{ant} will shift the optimum point to the right, yielding a higher optimal frequency of operation.

6

Conclusion

Energy harvesting within the body is an interesting research topic, the outcome of which could potentially enable a whole new range of applications from biomedical implants, self-locomotive biomedical sensors to touch skin interface. As previously discussed, glucose fuel cell has emerged as one of the viable methods for the long-term powering of biomedical implants due to its reliability, safety and ready availability of glucose and oxygen as reactants within the body. This thesis has shown how to build such a glucose fuel cell device at the millimeter scale while demonstrating its power density performance of 0.34uW/cm^2, which is suitable for low-power application. In addition, we have also developed the concentration model that could enable the optimization of the fuel cell performance with regard to its dimensional parameters. Lastly, we have discussed the efficiency optimization of the power amplifier that is part of any simple wireless communication system normally found in such low-power applications of the glucose fuel cell.

In the future, this work could be expanded upon by improving the fuel cell power density performance with the use of better-performance anode and cathode. The assembly and construction method of the cell could be improved upon to provide better sealing of the cell. In addition, the system integration of the miniature glucose fuel cell with the associated electronics should be further explored.

7

Appendix

7.1 First 1 CM^2 Prototype

Figure 7.1 shows the original 1cm^2 prototype, which uses two parts for assembly and hence requires additional fastening.

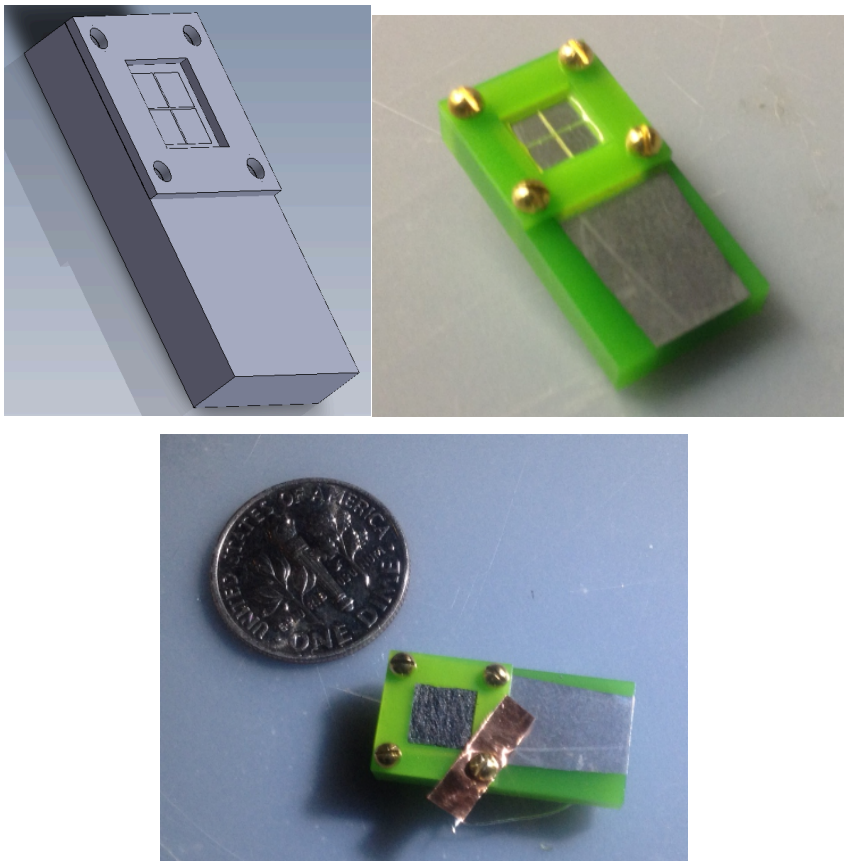

Figure 7.1 First 1cm^2 Prototype

7.2 Second 1 CM² Prototype

Figure 7.2 shows the second 1cm^2 prototype, which requires only one continuous part for the casing.

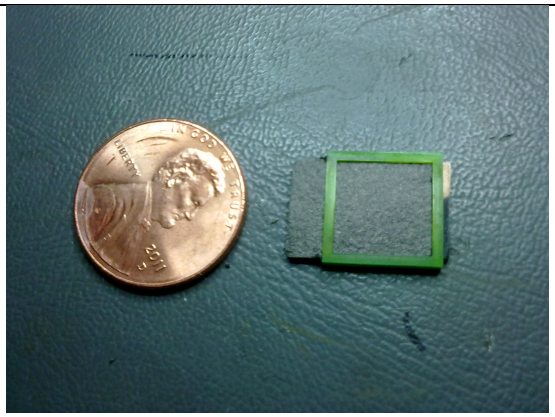

Figure 7.2 Second 1cm^2 Prototype

7.3 Full Derivation for the Optimization of the Power Amplifier

To maximize the efficiency, we want to minimize

$$A = (1 + R_S/R_{rad})(1 + 2\times C_g \times f_{osc} \times (R_{rad} + R_S))$$

First, let's consider the simplest case where the frequency has been chosen and we want to maximize the efficiency of the power amplifier by optimizing the width of the power transistor.

Substituting in the expression for Cg and Rs in term of W, we obtain:

$$A = (1 + R_{SW}/(W \cdot R_{rad}))(1 + 2\times C_{gate} \times W \times f_{osc} \times (R_{rad} + R_{SW}/W))$$

$$A = (1 + \frac{R_{SW}/R_{rad}}{W})(1 + 2\times C_{gate} \times W \times f_{osc} \times R_{rad} + 2\times C_{gate} \times f_{osc} \times R_{SW})$$

Taking the derivative of A with respect to W and simplifying, we have:

$$\frac{\partial A}{\partial W} = 0 = -\frac{\frac{R_{SW}}{R_{rad}}}{W^2} \times \left(1 + 2\times C_{gate} \times W \times f_{osc} \times R_{rad} + 2\times C_{gate} \times f_{osc} \times R_{SW}\right)$$

$$+(1 + \frac{R_{SW}/R_{rad}}{W}) \times 2 \times C_{gate} \times f_{osc} \times R_{rad}$$

$$0 = -\frac{R_{SW}}{R_{rad}} \times \left(1 + 2\times C_{gate} \times f_{osc} \times R_{SW}\right) + W \times 2 \times W \times C_{gate} \times f_{osc} \times R_{rad}$$

Thus, the optimal width is given by

$$W = \sqrt{\frac{R_{SW} \times \left(1 + 2\times C_{gate} \times f_{osc} \times R_{SW}\right)}{2\times C_{gate} \times f_{osc} \times R_{rad}^2}}$$

If the antenna is of the small electric dipole variant, the complete expression for W is

$$W = \sqrt{\frac{R_{SW} \times \left(1 + 2\times C_{gate} \times f_{osc} \times R_{SW}\right)}{2\times C_{gate} \times f_{osc}^5 \times R_k^2}}$$

For the second case, we assume that the frequency has not been chosen and is also one of the optimization variables. We now also take into consideration the antenna loss resistance R_{ant} which is the Ohmic loss due to the resistance of the metal that constitute the antenna (which is different from the radiation resistance R_{rad}). The expression for A then becomes:

$$A = 1 + 2\times C_g \times f_{osc} \times (R_{rad} + R_{ant} + \frac{R_{SW}}{W}) + \frac{R_{ant}+\frac{R_{SW}}{W}}{R_{rad}} + 2\times \frac{R_{ant}+\frac{R_{SW}}{W}}{R_{rad}} \times C_g \times f_{osc} \times (R_{rad} + R_{ant} + \frac{R_{SW}}{W})$$

(A quick way to obtain this is to substitute $R_{ant} + \frac{R_{SW}}{W}$ for R_s in the original expression for A.)

Simplifying this expression, we obtain:

$$A = 1 + 4\times C_{gate} \times f_{osc} \times R_{SW} + \frac{R_{ant}}{R_{rad}} + 4\times \frac{R_{SW}\times R_{ant}}{R_{rad}} \times C_{gate} \times f_{osc} + W\times[2\times C_{gate} \times f_{osc} \times (R_{rad} + R_{ant}) + 2\times R_{ant} \times C_{gate} \times f_{osc} + 2\times \frac{{R_{ant}}^2}{R_{rad}} \times C_{gate} \times f_{osc}] + \frac{1}{W} \times [\frac{R_{SW}}{R_{rad}} + 2\times \frac{{R_{SW}}^2}{R_{rad}} \times C_{gate} \times f_{osc}]$$

Using the Arithmetic Mean-Geometric Mean (AM-GM) inequality, we have

$$A \geq 1 + 4\times C_{gate} \times f_{osc} \times R_{SW} + \frac{R_{ant}}{R_{rad}} + 4\times \frac{R_{SW}\times R_{ant}}{R_{rad}} \times C_{gate} \times f_{osc} + 2\sqrt{\frac{R_{SW}}{R_{rad}} \times [1 + 2\times C_{gate} \times f_{osc} \times R_{SW}] \times 2 \times C_{gate} \times f_{osc} \times [R_{rad} + 2R_{ant} + \frac{{R_{ant}}^2}{R_{rad}}]}$$

Simplifying the expression, we get:

$$= \left(1 + \frac{R_{ant}}{R_k \times {f_{osc}}^2}\right)\left\{1 + 4 \times C_{gate} \times f_{osc} \times R_{SW} + 2\sqrt{2 \times C_{gate} \times f_{osc} \times R_{SW}\left[1 + 2 \times C_{gate} \times f_{osc} \times R_{SW}\right]}\right\}$$

To simplify further, let x = $2 \times C_{gate} \times f_{osc} \times R_{SW}$, the expression then becomes

$$A(x) = \left(1 + \frac{R_{ant} \cdot 4 \cdot {C_{gate}}^2 \cdot {R_{SW}}^2}{R_k \cdot x^2}\right)\left\{1 + 2x + 2\sqrt{x + x^2}\right\}$$

$$= \left(1 + \frac{m}{x^2}\right)\left\{1 + 2x + 2\sqrt{x + x^2}\right\}$$

where m is a constant. The expression can then be minimized numerically to obtain the optimum value for x, which corresponds to an optimum value for f_{osc}.

References

[1] L. R. Hochberg et al., “Neural ensemble control of prosthetic devices by a human with tetraplegia”, *Nature*, vol. 442, pp.164-171, July 2006.

[2] K. Wise et al., “Wireless implantable microsystems: high-density electronic interfaces to the nervous system”, *Proceedings of the IEEE*, vol. 92, pp. 76-97, 2004.

[3] Muller, Rikky, Simone Gambini, and Jan M. Rabaey. "A 0.013 mm 2 5μW DC-coupled neural signal acquisition IC with 0.5 V supply." *Solid-State Circuits Conference Digest of Technical Papers (ISSCC), 2011 IEEE International*. IEEE, 2011.

[4] Baker, Michael Warren, and Rahul Sarpashkar. *A low-power cochlear implant system*. Diss. Massachusetts Institute of Technology, 2007.

[5] M. Koplow et al., “Thick film thermoelectric energy harvesting systems for biomedical applications”, Proceeding of the 5th International Workshop on Wearable and Implantable Body Sensor Network, China, pp. 322-325, 2008.

[6] Z. Li et al., “Muscle-driven in vivo nanogenerator”, Advanced Materials, vol. 22 (23), pp. 2534-2537, 2010.

[7] Rabaey, Jan M., et al. "Powering and communicating with mm-size implants." *Design, Automation & Test in Europe Conference & Exhibition (DATE), 2011*. IEEE, 2011.

[8] Oncescu, Vlad, and David Erickson. "A microfabricated low cost enzyme-free glucose fuel cell for powering low-power implantable devices." *Journal of Power Sources* 196.22 (2011): 9169-9175.

[9] Kerzenmacher, S., et al. "A potentially implantable glucose fuel cell with Raney-platinum film electrodes for improved hydrolytic and oxidative stability." *Journal of Power Sources* 196.3 (2011): 1264-1272.

[10] Rapoport, Benjamin I., Jakub T. Kedzierski, and Rahul Sarpeshkar. "A Glucose Fuel Cell for Implantable Brain–Machine Interfaces." *PloS one* 7.6 (2012): e38436.

[11] H. Warner and B.W. Robinson, “A glucose cell”, *Digest of the 7th International Conference on Medical and Biological Engineering, Stockholm*, Sweden, p. 520., 1967.

[12] “Typical Half-Cell Diagram”, 7 Dec 2012 <http://www.chegg.com/homework-help/questions-and-answers/diagram-shows-typical-cell-containing-standard-half-cells-cell-operates-according-equation-q1325460>

[13] H.P Le and Z. Iqbal, “1mm3 Implantable communication and display systems powered by bio-fuel cells”, *Qualcomm Innovation Fellowship Finalist Presentation.* 2011.

[14] Wheeler, Harold A. "Fundamental limitations of small antennas." *Proceedings of the IRE* 35.12 (1947): 1479-1484.

[15] Heller, Adam. "Miniature biofuel cells." *Phys. Chem. Chem. Phys*. 6.2 (2003): 209-216.

[16] Bradley, David. "Fuelling the future." *Education in Chemistry*. (2006).